IEEE Open Journal of
Power Electronics

Received 23 April 2024; revised 20 May 2024; accepted 24 May 2024. Date of publication 28 May 2024;
date of current version 11 June 2024. The review of this article was arranged by Associate Editor Qiang Wei.

Digital Object Identifier 10.1109/OJPEL.2024.3406428

Uncertainty-Informed Threshold Assessment of Model-Based Fault Detection for Modular Multilevel Converters

YANTAO LIAO [1], YI ZHANG [2] (Member, IEEE), JUN YOU [1], LONG JIN [1], ZHIKE XU [1], AND ZHAN SHEN [1] (Member, IEEE)

[1]Department of Electrical Engineering, Southeast University, Nanjing 210096, China
[2]AAU Energy, Aalborg University, 9220 Aalborg, Denmark

CORRESPONDING AUTHOR: YI ZHANG (e-mail: yiz@energy.aau.dk).

This work was supported in part by the National Natural Science Foundations of China under Grant 52207191, in part by the Nanjing Science and Technology Innovation project for overseas students under Grant 4216002303, and in part by the Start-up Research Fund of Southeast University under Grant RF1028623299.

ABSTRACT Determining threshold values in model based fault detection (MBFD) is a longstanding challenge, which is often addressed through empirical and ambiguous adjustments. To tackle this issue, this paper proposes an uncertainty-informed framework for quantitative threshold assessment. The framework comprises three stages: 1) identifying uncertainties by explicitly understanding the implemented MBFD method, 2) quantifying fault detection residual through uncertainty propagation, and 3) determining and optimizing threshold values based on the quantified misdiagnosis rates. To validate the effectiveness of the proposed approach, a case study of a modular multilevel converter is selected. The proposed method not only enables a quantified threshold assessment but also enhances the robustness of the fault detection by accounting for uncertainties.

INDEX TERMS Model-based fault detection, modular multilevel converters, uncertainty quantification, threshold assessment.

I. INTRODUCTION

Fault detection plays a pivotal role in ensuring the reliable operation of modular multilevel converters (MMCs). With the increasing utilization of MMCs in safety-critical applications such as renewable energy [1], motor drive [2], and power transmissions [3], the failure of MMCs has become increasingly severe. Timely and robust fault detection is vital to mitigate these risks and ensure the continued reliability of these systems.

Among the various fault detection approaches, such as signal-based [4] and data-driven solutions [5], model-based fault detection (MBFD) techniques are widely used for MMCs as their system behaviors and dynamics can be modeled with high accuracy differential equations [6]. This characteristic not only ensures an effective fault detection but also offers superior generality as it does not rely on additional sensing systems. In general, MBFD compare the output of a mathematical model to measured quantities of the system to generate a residual which acts as a fault indicator. Ideally, the residual should be zero when the system is healthy and deviate from zero when a fault is present. However, the impact of uncertainties results in a nonzero residual even when no fault is present, necessitating the selection of an appropriate threshold. As shown in Fig. 1, Conservative decisions can generate more false alarms, leading to operational interruptions and significant losses, which are highly undesired for

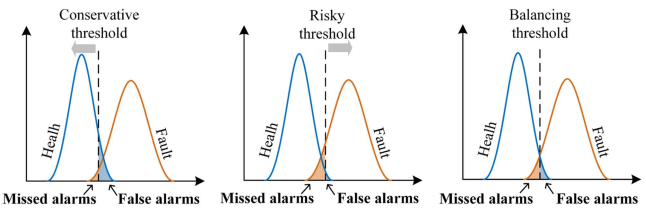

FIGURE 1. Missed alarms and false alarms under various thresholds in an MBFD method.

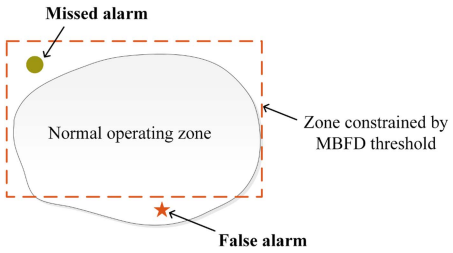

FIGURE 2. Potential outcomes of MBFD implementation.

applications such as wind generation and power transmission [7], [8]. Conversely, missed alarms increase when a risky threshold is applied, posing severe risks in domains like aerospace [9]. It is impossible to decrease false alarms and missed alarms simultaneously by adjusting the threshold. Hence, the threshold needs to be chosen large enough to eliminate false alarms, yet small enough to ensure failures are detected. How to select a balancing threshold is a trade-off to be considered.

Typically, a threshold is set manually based on experimental tests and practical engineering experience. [10], [11], [12], [13]. In [3], multiple manual thresholds are designed to improve the robustness of MBFD against uncertainties. Compared with the manual methods, an adaptive threshold method shows robust performance under varying load conditions [14]. With the rapid development of computing technology, machine learning method has been introduced to generate threshold [15], [16]. These threshold selection approaches find the compromise solution under a few deterministic scenario tests that do not reflect to the stochastic nature of the system states. The results cannot provide the risk measurement under various thresholds since they do not quantify uncertainties in the MBFD system. They are not able to find the best solution when the decision-maker's preferences are changed.

On the other hand, the inherent uncertainties and associated risks have not received adequate attention. The existing studies often provide validations as having seemly 100% accuracy of detecting faults [17]. These validations are carried out based on one or a few specified scenarios representing parameters variations or power changes, which are very common in MMCs. Without explicitly considering uncertainties, MBFD methods that perform well under ideal laboratory conditions may fall short in real-world applications. As shown in Fig. 2, while a fault is easily detected by a preset MBFD threshold with considering ideal laboratory conditions, the practical implementations subject to various uncertainties are possible to generate false alarms and missed alarms. For example, numerous false alarms and a detection rate of less than 25% for faults in wind applications are substantially challenging for the industry [7]. Hence, the consideration of uncertainties and the evaluation of their impacts at a system-level are crucial. These root-cause understandings serve as prerequisites for the reasonable threshold setting of MBFD methods.

Recently, considering that uncertainties are in their nature random variables, the probabilistic framework has been developed in MMCs, such as reliability assessment [18], modeling design [19], and early failure analysis [20]. However, connecting stochastic uncertainties, risk and threshold assessment within a unified probabilistic framework remains under exploited, especially for the MBFD systems of MMCs.

In this paper, we propose a probabilistic framework to assess threshold considering uncertainties and to provide a targeted optimization based on the assessment results. The framework mainly consists of three elements: uncertainty investigation, uncertainty propagation, and threshold assessment. To illustrate the practical application of the proposed framework, an in-depth analysis of a sub-module (SM) open-circuit MBFD method [13] is conducted. The uncertainty investigation stems from a clear understanding for the MBFD system. Considering the coupling effects of multiple uncertainty factors, the framework enables a quantitative threshold assessment through the Monte Carlo method. Leveraging two comprehensive evaluation metrics, the threshold can be set based on specific risk decision-making, achieving a trade-off between the false alarm rate and the missed alarm rate.

II. THE PROPOSED METHODOLOGY

The main idea and the steps of the proposed framework are presented in this section.

A. THRESHOLD ASSESSMENT CONSIDERING UNCERTAINTIES AND RISKS

We consider an MBFD system whose residual is defined as ε, expressed in the form:

$$\varepsilon = h(x) \tag{1}$$

where h represents the function which describe the MBFD under study, x is a multidimensional input variable.

The MBFD's residual is affected by different categories of uncertainties, including model parameter mismatch (caused by manufacturing tolerance, degradation, etc.), measurement accuracy, varied operational conditions, etc. To model these uncertainties, an uncertainty factor $\delta_x \in \mathbb{R}^+$ is defined as

$$\tilde{x} = \delta_x \cdot x \tag{2}$$

where $\tilde{x}$ represents the practical input considering uncertainties.

Then, the residual considering uncertainties can be formulated as

$$\tilde{\varepsilon} = h(\tilde{x}) \tag{3}$$

where $\tilde{\varepsilon}$ represents the residual with uncertainties.

Given a threshold ε_{th}, the false alarm probability P_{FA} and fault detection probability P_{FD} are expressed as

$$P_{\text{FA}} = \text{P}_\text{r}\left\{\tilde{\varepsilon} > \varepsilon_{\text{th}} \,|\text{Health}\right\} = E\left[I_1\left\{\tilde{\varepsilon} > \varepsilon_{\text{th}}\right\}\right] \tag{4}$$

$$P_{\text{FD}} = \text{P}_\text{r}\left\{\tilde{\varepsilon} > \varepsilon_{\text{th}} \,|\text{Fault}\right\} = E\left[I_2\left\{\tilde{\varepsilon} > \varepsilon_{\text{th}}\right\}\right] \tag{5}$$

where $\mathrm{P_r}\{\cdot\}$ is the event probability, $E[\cdot]$ is the expectation, I is the indicator function, and

$$I\{\tilde{\varepsilon} > \varepsilon_{\mathrm{th}}\} = \begin{cases} 1, & \tilde{\varepsilon} > \varepsilon_{\mathrm{th}} \\ 0, & \tilde{\varepsilon} \leqslant \varepsilon_{\mathrm{th}} \end{cases} \tag{6}$$

$\tilde{\varepsilon}$ is sometimes complicated function of $\tilde{x}$. It is difficult to obtain a closed-form solution for (4) and (5). Based on the law of large numbers, Monte Carlo simulation generates a large number of samples and calculates the mean of $I_1\{\tilde{\varepsilon} > \varepsilon_{\mathrm{th}}\}$ and $I_2\{\tilde{\varepsilon} > \varepsilon_{\mathrm{th}}\}$ to approximate the expectation. Accordingly, P_{FA} and P_{FD} can be expressed as

$$P_{\mathrm{FA}} = \frac{1}{n}\sum_{i=1}^{n} I_1\{\tilde{\varepsilon}_i > \varepsilon_{\mathrm{th}}\} \tag{7}$$

$$P_{\mathrm{FD}} = \frac{1}{n}\sum_{i=1}^{n} I_2\{\tilde{\varepsilon}_i > \varepsilon_{\mathrm{th}}\} \tag{8}$$

where $\tilde{\varepsilon}_i$ is the i-th residual sample and n is the sample size.

We always expect that P_{FA} is the lower the better and P_{FD} is the higher the better. The trade-off between P_{FA} and P_{FD} by selecting a suitable $\varepsilon_{\mathrm{th}}$ ensures a good performance of MBFD methods. Upon a risk decision-making, $\varepsilon_{\mathrm{th}}$ can be evaluated sequentially using the receiver operating characteristic (ROC) curve and F-measure score [21]. The ROC curve is formed by plotting P_{FD} over P_{FA}, and any point in the ROC curve corresponds to the performance of the MBFD method on a given $\varepsilon_{\mathrm{th}}$. It provides a graphical representation that intuitively reveals the trade-offs between benefits (reflected by P_{FD}) and costs (reflected by P_{FA}) at various thresholds.

As we mainly focus on the quantitative assessment of the MBFD under various thresholds, F-measure score is introduced, which is defined as

$$F_\beta = \frac{(1+\beta^2)P_{\mathrm{FD}}}{\beta^2(P_{\mathrm{FD}} + P_{\mathrm{FA}}) + 1} \tag{9}$$

where β is a coefficient to adjust the relative importance of P_{FA} versus P_{FD}, which is commonly varied between 0.5 and 2 by risk decision-making [22]. $\beta = 1$ means equal importance. The smaller β, the more important P_{FD} and vice versa.

Setting a reasonable threshold can achieve trade-offs of P_{FA} and P_{FD} to some extent. However, it is not possible to reduce P_{FA} while increase P_{FD}. Further optimization is needed if any threshold cannot meet the performance requirements for MBFD methods. This requires sensitivity analysis to investigate and eliminate the dominant uncertainty factors that impact the residual. Based on this idea, a tailored optimization strategy can be designed.

B. STEPS OF THE PROPOSED FRAMEWORK

The proposed framework is composed of the following main steps:

1) Investigate uncertainty factors δ_x caused by model parameter mismatch, measurement accuracy, and varied operational conditions, etc. Derive the residual expression that includes uncertainties.
2) Obtain the distribution of residual $\tilde{\varepsilon}$ using Monte Carlo simulation.
3) Plot the ROC curve and calculate F_β with various $\varepsilon_{\mathrm{th}}$.
4) Perform a sensitivity analysis between residual and uncertainty factors. Optimize the MBFD method by eliminating the main uncertainty factors.
5) Repeat steps 2 and 3 to reevaluate $\varepsilon_{\mathrm{th}}$.

Fig. 3 shows the flow charts for the proposed framework. It should be noted that steps 4 and 5 are not mandatory, and it is recommended to perform them when the original MBFD method fails to meet the performance requirements.

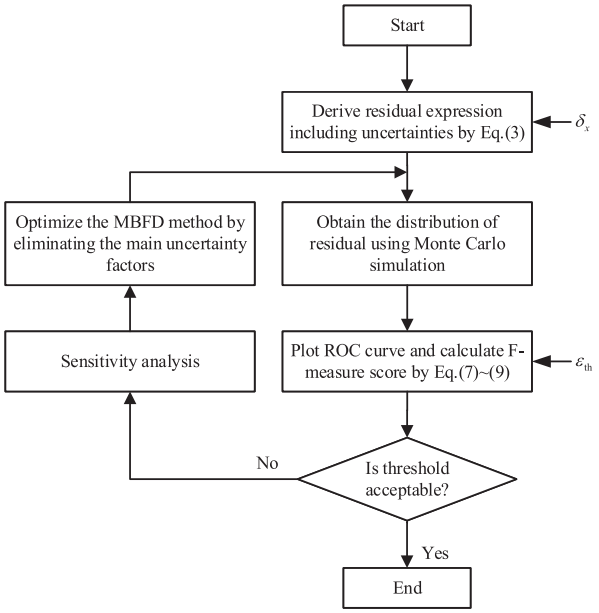

FIGURE 3. Flow chart for the proposed framework for threshold assessment.

III. A MOTIVATING CASE STUDY OF THE MMC

In this section, an existing MBFD method [13] for detecting SM open-circuit faults in MMC is employed as a motivating case. Reference [13] has preset a threshold of 0.8 by robustness tests. However, a clear methodology for modeling uncertainties and assessing thresholds systematically is lacking.

A. AN ESTABLISHED MBFD METHOD

The topology structure of a three-phase MMC and its SM are shown in Fig. 4. It consists of six arms, where each arm contains N series-connected SMs and an arm inductor. Take phase a as an example and the subscript is neglected for simplification. Here, L_0 represents the arm inductance (the upper and lower arm inductance are also denoted as L_p and L_n to consider their differences); $u_{c,i}$ represents the capacitor voltage of the i-th $(1, 2, \ldots, 2N)$ SM; i_p and i_n represent the currents of the upper and lower arms; u_p and u_n represent the voltages of the upper and lower arms; U_{dc} and i_{dc} represent the voltage and current on the dc bus; u_{ac} and i_g represent the ac-side voltage and current, respectively; $\mathrm{T_1}$ and $\mathrm{T_2}$ are the

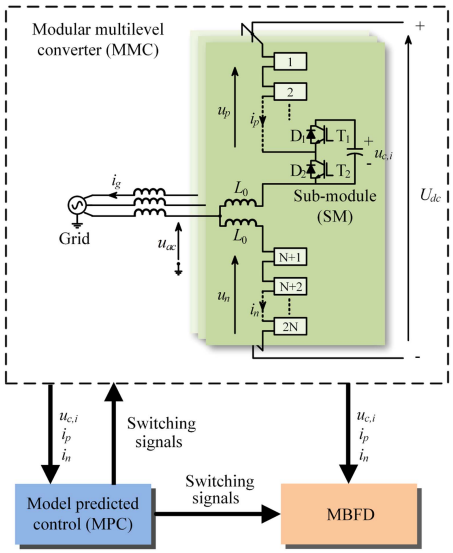

FIGURE 4. Topology structure of an MMC and an existing MBFD method [13] for open-circuit fault detection based on model predictive control.

two power switching devices of the SM, while D_1 and D_2 are the corresponding anti-parallel diodes.

Open-circuit failure of the IGBTs in SMs is a significant issue due to its high failure contribution. Reference [13] proposed an MBFD approach based on a model predictive control (MPC) as shown in Fig. 4. Given the known switching states by the MPC controller, the open-circuit fault is detected by calculating the difference between the measured phase voltage and the estimated phase voltage. For instance, the measured phase voltage u_m and corresponding estimated phase voltage u_e can be expressed as

$$u_m = \sum_{i=1}^{2N} u_{\mathrm{sm},i} = \sum_{i=1}^{2N} S_i u_{c,i} \tag{10}$$

$$u_e = U_{dc} - L_0 \left(\frac{i_p^k - i_p^{k-1}}{T_s} + \frac{i_n^k - i_n^{k-1}}{T_s} \right) \tag{11}$$

where $u_{\mathrm{sm},i}$ and S_i are the output voltage and binary switching function of the i-th SM, respectively.

To ensure that the residual is not dependent on the SM capacitor voltage, the residual expression can be standardized as

$$\varepsilon = \frac{N(u_m - u_e)}{U_{dc}} \tag{12}$$

Ideally, the residual ε is zero if no fault while the one above zero is faulty. To consider practical uncertainties, an open-circuit fault can be identified when the residual satisfies $|\varepsilon| > \varepsilon_{\mathrm{th}}$. The threshold $\varepsilon_{\mathrm{th}}$ in [13] is selected as 0.8 and the experimental results have verified good effectiveness under the laboratory conditions, whether the empirical selection of the threshold performs a robust MBFD remains unknown. The following part will first conduct a theoretical derivation of the residual expression including uncertainties.

TABLE 1. Different Categories of Uncertainty Factors Affect the MBFD

Type	Parameter x	Practical value $\tilde{x}$ or notes
Parameter mismatch	L_0	$\tilde{L}_p = \delta_{L_p} L_0$ $\tilde{L}_n = \delta_{L_n} L_0$
Measurement accuracy	U_{dc} u_c i_p i_n	$\tilde{U}_{dc} = \delta_{U_{dc}} U_{dc}$ $\tilde{u}_c = \delta_{u_c} u_c$ $\tilde{i}_p = \delta_{i_p} i_p$ $\tilde{i}_n = \delta_{i_n} i_n$
Varied conditions	U_{dc}, i_g	e.g., step change, load variations
Deterministic parameter	N, T_s	enhancing or attenuating uncertainties

B. UNCERTAINTY INVESTIGATION OF THE RESIDUAL

The uncertainties involved in (10), (11), and (12) are analyzed. The upper and lower arm inductance L_0 is subject to uncertainties cause by temperature, saturation and aging. The measurement accuracy of i_p, i_n, U_{dc}, and u_c have uncertainties. In addition to the steady state, the uncertainties also depend on the dynamics of U_{dc} and i_g which are related to the operational conditions. As shown in Table 1, these uncertainties are modeled based on (2). Substituting the uncertainty factors in Table 1, (10) and (11) can be rewritten as

$$\tilde{u}_m = \sum_{i=1}^{2N} \delta_{u_c} u_{\mathrm{sm},i} \tag{13}$$

$$\tilde{u}_e = \delta_{U_{dc}} U_{dc} - \delta_{L_p} L_0 \frac{\delta_{i_p}(i_p^k - i_p^{k-1})}{T_s} - \delta_{L_n} L_0 \frac{\delta_{i_n}(i_n^k - i_n^{k-1})}{T_s} \tag{14}$$

The residual with uncertainties is modeled as

$$\tilde{\varepsilon} = N \frac{\tilde{u}_m - \tilde{u}_e}{\tilde{U}_{dc}} \tag{15}$$

In particular, $\tilde{\varepsilon} = \varepsilon$ if all $\delta_x = 1$, indicating that the residual does not incorporate uncertainties. According to (13), (14) and (15), $\tilde{u}_m$ is affected by the uncertainty factors of δ_{u_c}. $\tilde{u}_e$ suffers from multiple uncertainty factors, such as $\delta_{U_{dc}}$, δ_{L_p}, δ_{L_n}, δ_{i_p}, δ_{i_n}, and the dynamics of U_{dc} and i_g which depend on operational conditions. Moreover, deterministic parameters such as N and T_s also affect the residual by enhancing or attenuating uncertainties.

IV. THRESHOLD ASSESSMENT BASED ON MONTE CARLO

Analytical model is difficult to give quantitative results of the uncertainty propagation, in particular of considering the coupling effects of different uncertainties and dynamic conditions simultaneously. To address this problem, this section employs Monte Carlo analysis to obtain the distribution of residual. Further, the quantitative evaluation of the threshold is achieved.

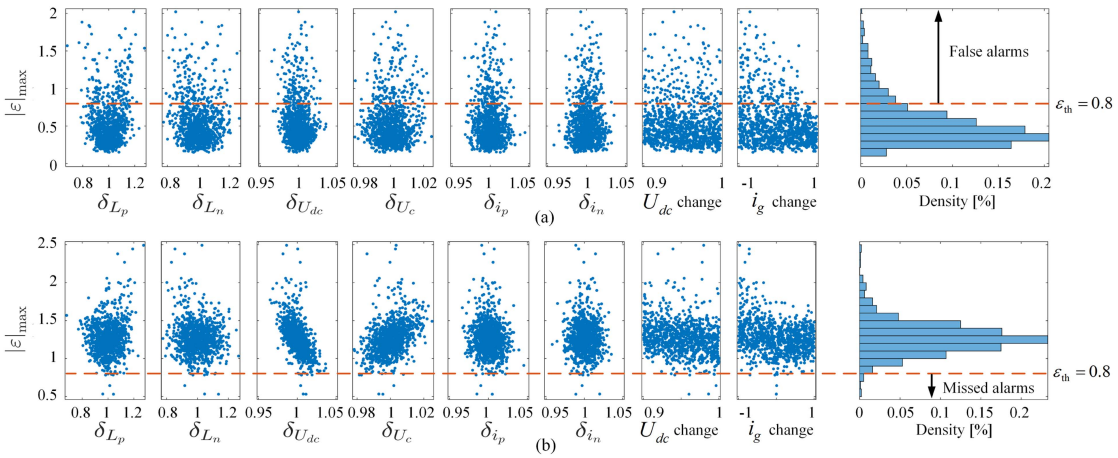

FIGURE 5. Distributions of the residual under health and fault states: (a) health state; (b) fault state.

TABLE 2. Uncertainty Factors Distributions

Parameters	Nominal Value	Variation Range	Distribution	References
δ_{L_p}, δ_{L_n}	1	$[0.8, 1.2]$	Normal	[23]
$\delta_{U_{dc}}$	1	$[0.97, 1.03]$	Normal	[24]
δ_{u_c}	1	$[0.98, 1.02]$	Normal	[25]
δ_{i_p}, δ_{i_n}	1	$[0.97, 1.03]$	Normal	[26]
U_{dc}	1 p.u.	[0.9 p.u., 1 p.u.]	Uniform	[27]
i_g	1 p.u.	[−1 p.u., 1 p.u.]	Uniform	-

TABLE 3. Main Circuit Parameters of the MMC for Monte Carlo Analysis

Parameters	Values	Units
Rated power	1.2	MW
The ac side current	100	A
The dc bus voltage	20	kV
Arm inductance	20	mH
Line frequency	50	Hz
Number of SMs per arm	10	-
SM capacitance	2000	μF
SM capacitor voltage	2000	V
Sampling and control period	20	μs

A. MONTE CARLO SIMULATION

Monte Carlo method estimate the distribution of the residual by simulating the actual process and random behavior of the system. The method treats the problem as a series of simulations. This is achieved in two steps: random variate generation and random system state simulation.

Reasonable variations of uncertainty factors are strictly followed by practical conditions and the existing literature, which are given in Table 2. The inductance mismatch and measurement accuracy are independent random factors that tend to be in a normal distribution according to the central limit theorem. Whereas, the operational variations are not purely random issues, which are regarded as a uniform distribution. The nominal parameters of the analyzed MMC system are listed in Table 3. Then, 1000 random samples are generated and the distributions of residual under health and fault states are shown in Fig. 5. Here, $|\varepsilon|_{\max}$ is the maximum fluctuation of the residual. Take the threshold of 0.8 in [13] as an example, Fig. 5(a) shows that although the residual is largely concentrated within the defined threshold, the residual exceeds the threshold in 153 samples out of 1000 samples. Specifically, as δ_{L_p} and δ_{L_n} deviate more from 1, $|\varepsilon|_{\max}$ tends to increase, indicating a more severe inductance mismatch and larger residual fluctuation. It is also observed that even when δ_{L_p} and δ_{L_n} are close to 1, $|\varepsilon|_{\max}$ can still possibly fall into a region with larger values. It means that the inductance mismatch is not the only factor affecting the residual. Obviously, $|\varepsilon|_{\max}$ tends to beyond the threshold when i_g changes from 1 p.u. to -1 p.u.. This is attributed to the power step rapidly, thereby causing an increase in the residual.

On the contrary, when the MMC has an open-circuit fault, Fig. 5(b) shows among the 1000 samples, 992 samples have a residual greater than 0.8, and only 8 faults are missed in the detection. In fault state, the faults can be detected when the residual exceeds the threshold. Thus, δ_{L_p}, δ_{L_n} and i_g, which cause the residual to be larger, no longer influence the outcomes. In addition, a clear correlation between measurement accuracy and the residual can be observed. For instance, if $\delta_{U_{dc}}$ is larger and δ_{u_c} is lower, $|\varepsilon|_{\max}$ tend to shift downwards, which may result in missed alarms.

According to the above analysis, it also can be seen that ε_{th} plays a vital role in the misdiagnosis risk. For example, increasing ε_{th} may be able to reduce false alarms but at the cost of increasing the missed alarms. Thus, more in-depth analysis for the threshold assessment is required.

B. THRESHOLD ASSESSMENT WITH ROC CURVE AND F-MEASURE SCORE

For overall threshold assessment and comparison, the ROC curve and F-measure score are conducted. Fig. 6 shows the ROC curve which is fitted by a series of thresholds. Each point on the ROC curve corresponds to a value of the threshold. It

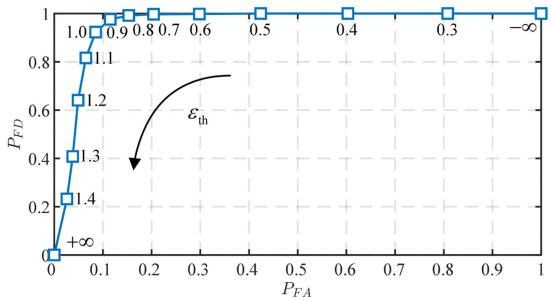

FIGURE 6. ROC curve of the MBFD with various thresholds.

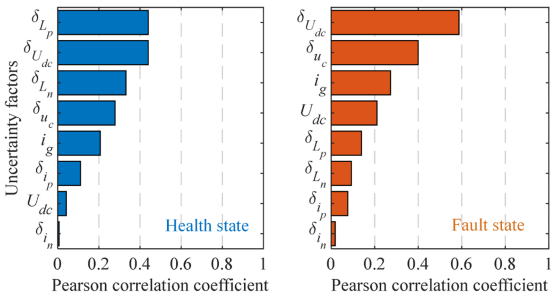

FIGURE 7. Pearson correlation coefficients between the residual and uncertainty factors: (a) health state; (b) fault state.

TABLE 4. F-Measure Score With Various Thresholds

ε_{th}	$P_{FA}(\%)$	$P_{FD}(\%)$	F_1	$F_{0.5}$	F_2
0.5	42.4	100	0.8251	0.9218	0.7467
0.8 ([13])	15.3	99.2	0.9250	0.9640*	0.8889
0.9	11.5	97.6	0.9335*	0.9586	0.9098
1.0	8.5	92.3	0.9193	0.9215	0.9172*
2.1	< 0.1	0.4	0.0080	0.0050	0.1970

provides a graphical representation of the relative trade-offs between P_{FA} and P_{FD}.

Table 4 lists the F-measure score with various thresholds. $\varepsilon_{th} = 0.8$ denotes the default value in [13], which achieves the optimal choice by highlighting P_{FD}. However, when more importance is given to P_{FA} than to P_{FD}, the optimal threshold is achieved at $\varepsilon_{th} = 1.0$. Considering equal importance between P_{FA} and P_{FD}, $\varepsilon_{th} = 0.9$ is preferred. In addition, the MMC system is always expected to avoid false alarms due to the expensive maintenance cost. Thus, a P_{FA} requirement is set as $P_{FA} < 0.1\%$ for reference, which corresponds to $\varepsilon_{th} = 2.1$ and $P_{FD} = 0.4\%$. As a supplement, $\varepsilon_{th} = 0.5$ denotes a $P_{FD} = 100\%$ at the expense of $P_{FA} = 42.4\%$. In summary, the results provide the quantitative trade-offs between risks and benefits.

Threshold assessment reveals the misdiagnosis risks of the MBFD with considering uncertainties. It implies that shifting ε_{th} is limited to improve the overall MBFD performance based on the two contrasting misjudgment risks. Thus, a root-cause analysis is a prerequisite to optimize the MBFD.

V. AN OPTIMIZATION SOLUTION BASED ON SENSITIVITY ANALYSIS

Targeted optimization needs to find the leading uncertainty factors. Sensitivity analysis is applied first in this section. Then, an inductance estimation method is used to eliminate the dominant uncertainties. Finally, the Monte Carlo analysis is conducted to reevaluate the thresholds.

A. SENSITIVITY ANALYSIS AND UNCERTAINTY ELIMINATION

The correlations between the residual and uncertainty factors are computed by Pearson correlation coefficient ρ_{XY}, which is given by

$$\rho_{XY} = \frac{\left|\sum_{i=1}^{n}\left(X_i - \bar{X}\right)\left(Y_i - \bar{Y}\right)\right|}{\sqrt{\sum_{i=1}^{n}\left(X_i - \bar{X}\right)^2 \cdot \sum_{i=1}^{n}\left(Y_i - \bar{Y}\right)^2}} \tag{16}$$

where X are the inputs (e.g. uncertainty factors), Y are the outputs (e.g. residuals), $\bar{X}$ and $\bar{Y}$ are the corresponding average values. The value of ρ_{XY} has a range from 0 to 1, where a larger value indicates a stronger correlation.

Fig. 7 shows the Pearson correlation coefficients between the residual and uncertainty factors in health and fault states, respectively. Firstly, δ_{L_p} and δ_{L_n} significantly affect the residual in health state. This parameter mismatch is one of the leading factors resulting in false alarms. Next, the measurement accuracy in particular of $\delta_{U_{dc}}$ and δ_{u_c} plays a vital role in both health and fault states. Thus, the subsequent research hypothesis is that if more accurate voltage sensors are employed, the MBFD method can have a better performance. Moreover, arm inductance mismatch as a leading factor in health state is difficult to improve by upgrading hardware. To address this issue, a targeted optimization solution using an observer [28] is employed to estimate the upper and lower arm inductance. The detailed derivation is included in Appendix. Then, the estimated phase voltage $\hat{u}_e$ and the corresponding residual $\hat{\varepsilon}$ can be rewritten as

$$\hat{u}_e = U_{dc} - \hat{L}_p \frac{i_p^k - i_p^{k-1}}{T_s} - \hat{L}_n \frac{i_n^k - i_n^{k-1}}{T_s}, \tag{17}$$

$$\hat{\varepsilon} = \frac{N(u_m - \hat{u}_e)}{U_{dc}}. \tag{18}$$

where $\hat{L}_p$ and $\hat{L}_n$ are the estimated upper and lower arm inductance, respectively.

By estimating the upper and lower arm inductance online, the effects of dominant uncertainty factors on the residual can be suppressed.

B. MONTE CARLO SIMULATION OF THE IMPROVED MBFD METHOD

To compare the performance between the original MBFD method and the improved one, the Monte Carlo analysis and threshold assessment are conducted with identical 1000 samples in Section IV.

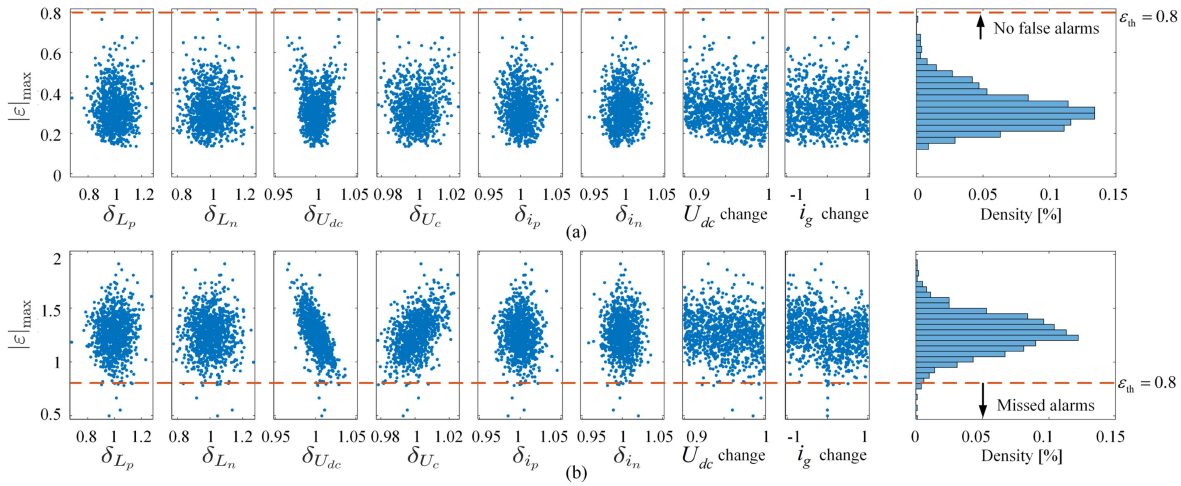

FIGURE 8. Distributions of the residual for the improved MBFD method under health and fault states: (a) health state; (b) fault state.

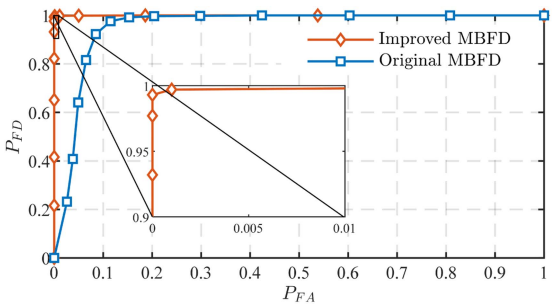

FIGURE 9. Comparison of ROC curves between the original and the improved MBFD methods.

Fig. 8 shows the distributions of the residual for the improved MBFD method under health and fault states. In the health state, no sample exceeds the threshold. Furthermore, there is no significant trend in δ_{L_p}, δ_{L_n} and i_g, indicating that the improved MBFD system is no longer prone to false alarms caused by arm inductance mismatch and power step. In the fault state, owing to the weak correlation between inductance mismatch and the residual, the inductance estimation has almost no impact on the distributions of the residual. There are still 8 samples indicating that the residuals do not exceed the threshold.

C. THRESHOLD ASSESSMENT OF THE IMPROVED MBFD METHOD

In order to quantitatively compare the performance of both MBFD methods, one generally uses area under the curve (AUC) [29] as an evaluation criterion. In Fig. 9, the improved MBFD method achieves a higher AUC value of 0.9994, compared to the original method's AUC of 0.9532; therefore, the improved MBFD method can provide better overall performance.

Table 5 lists the F-measure score with various thresholds of the improved MBFD method. The F-measure score exhibits a general rise. Specifically, $\varepsilon_{\text{th}} = 0.4$ denotes $P_{\text{FD}} = 100\%$, and $P_{\text{FA}} = 18.6\%$ is much lower than the original MBFD method (42.4%). It is noteworthy that 0.7 is the optimal threshold regardless of risk preference. Considering a $P_{\text{FA}} < 0.1\%$ request for reference, $\varepsilon_{\text{th}} = 0.8$ is a better choice. In this case, P_{FD} is up to 99.3%, which is much better than the original MBFD method (0.4%).

TABLE 5. F-Measure Score With Various Thresholds of the Improved MBFD Method

ε_{th}	$P_{\text{FA}}(\%)$	$P_{\text{FD}}(\%)$	F_1	$F_{0.5}$	F_2
0.4	18.6	100	0.9149	0.9641	0.8705
0.7	0.1	99.7	0.9980*	0.9974*	0.9986*
0.8	< 0.1	99.3	0.9935	0.9944	0.9985

The inductance estimation achieves an optimization for the MBFD method. It is worth mentioning that the solutions should be varied based on specific evaluation results. The point is eliminating the effects of leading uncertainties on the residual. The quantified comparison between the original and the improved MBFD methods validates the effectiveness and feasibility of the uncertainty-informed threshold assessment for reducing misdiagnosis risks. Moreover, the F-measure score as a quantitative trade-off means provides a better threshold choice under uncertainties. It depends on the specific situation and demand.

VI. EXPERIMENTAL RESULTS

An 8-kVA MMC platform has been built for experimental verification, as shown in Fig. 10. Table 6 indicates the detailed parameters of the system. According to the quantified results of threshold assessment, the performance of the existing MBFD is severely degraded by a higher false alarm rate. Therefore, we focus on mitigating the false alarm problem caused by inductance mismatch and power change. Here, the

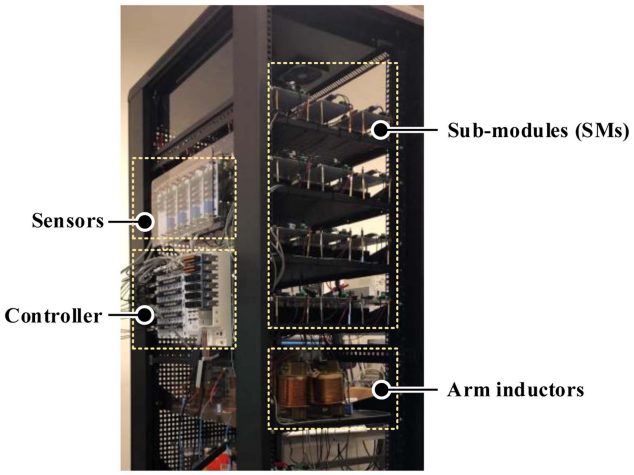

FIGURE 10. An 8-kVA MMC experimental platform.

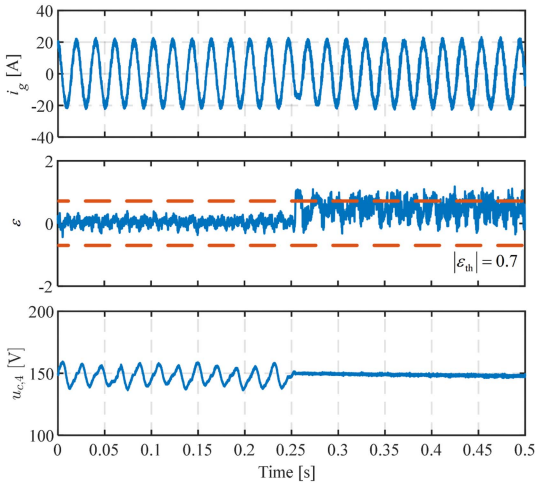

FIGURE 11. Experimental results of an open-circuit fault in 4th SM.

TABLE 6. Detailed Parameters of the MMC Experimental Platform

Parameters	Values	Units	Descriptions
The ac-side current	20	A	Nominal value
	5	A	Changed value
Arm inductance	5	mH	Nominal value
	4	mH	δ_{L_p} or $\delta_{L_n} = 0.8$
	6	mH	δ_{L_p} or $\delta_{L_n} = 1.2$
The dc bus voltage	600	V	Other factors
Number of SMs per arm	4	-	Other factors
SM capacitance	1640	μF	Other factors
SM capacitor voltage	150	V	Other factors
Sampling and control period	50	μs	Other factors

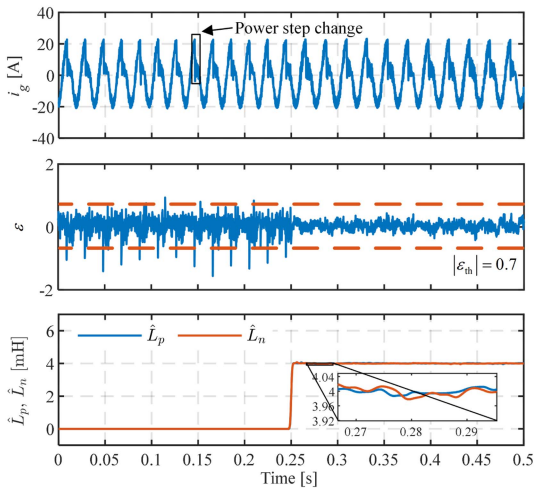

FIGURE 12. Experimental results with uncertainties: $\delta_{L_p} = \delta_{L_n} = 0.8$; i_g changes from 20 A to 5 A.

threshold of 0.7 is preferred by the quantified assessment in Table 5.

The IGBT open-circuit faults were generated by permanently inhibiting the corresponding gate signals to emulate the open-circuit fault. The experimental results of an open-circuit fault in 4th SM is shown in Fig. 11. During the health state, the residual stay within the threshold. However, when the open-circuit fault occurs at 0.25 s, the residual exceeds 0.7 rapidly, indicating that the fault is detected.

In health state, inductance mismatches and a power step change are involved, namely, $\delta_{Lp} = \delta_{Ln} = 0.8$, $\delta_{Lp} = 0.8$while$\delta_{Ln} = 1.2$, and $\delta_{Lp} = \delta_{Ln} = 1.2$. For example, $\delta_{Lp} = \delta_{Ln} = 0.8$ means that the actual inductance is 80% of the nominal inductance. Intentionally introducing a power step change by changing the ac-side current from 20 A to 5 A periodically, Fig. 12 shows the MBFD performance under $\delta_{Lp} = \delta_{Ln} = 0.8$. The residual exhibits extreme fluctuation before 0.25 s. It frequently exceeds the threshold, especially at the time of power step change, leading to false alarms. However, the inductance has been accurately estimated with the error below 4% after enabling the inductance estimation. The residual fluctuation is suppressed and the false alarms are eliminated.

Figs. 13 and 14 show the results when the upper and lower arm inductances are divergent and undervalued, respectively. Similarly, the residual fluctuation can be well suppressed under inductance mismatch and power step change.

VII. THRESHOLD ASSESSMENT OF STATE OF THE ARTS

To further highlight the threshold selection and quantified assessment on MBFD methods of MMCs, four additional cases [3], [11], [30], [31] are studied by the proposed framework. Although the effectiveness of these methods has been validated under specific simulation or experimental condition, the risk of misdiagnosis remain prevalent. The threshold determination is also ambiguous. As shown in Fig. 15, the ROC curves and the corresponding AUC present the overall performance under various thresholds for these MBFD methods. Moreover, the results of threshold assessment are

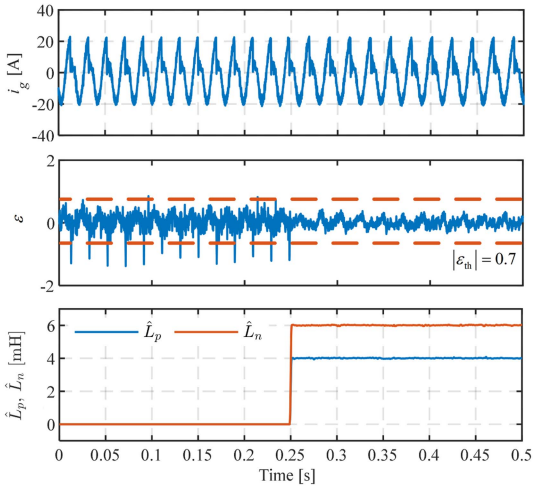

FIGURE 13. Experimental results with uncertainties: $\delta_{Lp} = 0.8$, $\delta_{Ln} = 1.2$; i_g changes from 20 A to 5 A.

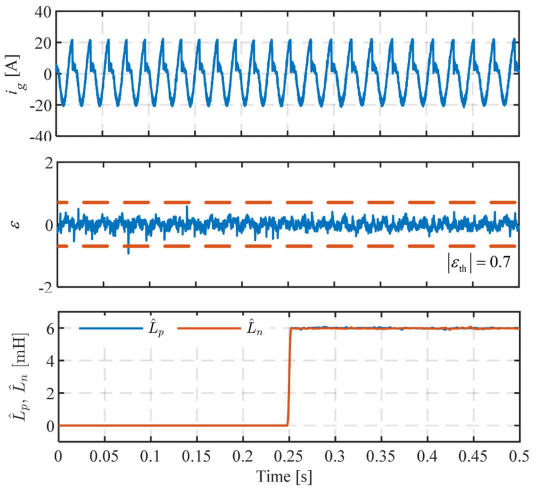

FIGURE 14. Experimental results with uncertainties: $\delta_{Lp} = \delta_{Ln} = 1.2$; i_g changes from 20 A to 5 A.

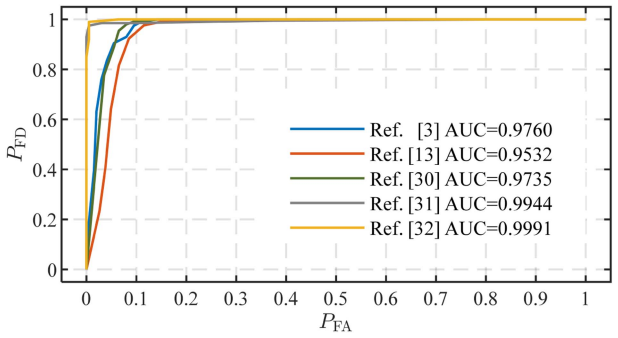

FIGURE 15. ROC curves and AUC of state of the arts.

listed in Table 7. Taking the top F_1 score as an example of decision-making preference, the preferred threshold and the corresponding misdiagnosis rate are given. It is worth noting that an MBFD method with a low AUC value could perform better at a specific threshold than an MBFD method with a high AUC value. For instance, although the AUC value of the method in [3] is higher than that of the method in [11], the performance at a specific threshold is the opposite.

TABLE 7. Threshold Assessment of State of the Arts

Ref.	Preferred threshold	P_{FA}(%)	P_{FD}(%)	F_1
[3]	0.8	11.0	99.0	0.9429
[13]	0.9	11.5	97.6	0.9335
[30]	1800	8.0	98.0	0.9514
[31]	16	0.5	97.5	0.9848
[32]	40	0.5	100	0.9975

VIII. CONCLUSION

This paper presented a statistics-based methodology instead of deterministic robust test to quantitatively assess the thresholds in MBFD for MMCs. An uncertainty-informed threshold assessment framework is proposed to model and propagate uncertainties, utilizing quantitative metrics for thresholds to achieve trade-offs between false alarms and missed alarms. A study case was successfully applied to validate the proposed framework. The coupling effects of multiple uncertainty factors are revealed based on Monte Carlo analysis. The threshold assessment with considering uncertainties is further achieved by ROC curve and F-measure score. The assessment results show that threshold adjustment is limited to improve the MBFD performance.

The overall performance of the studied MBFD method is improved by eliminating uncertainty factors. The comparative assessment underscore substantial enhancements of quantitative metrics under various thresholds. Experimental results also validate the feasibility of the uncertainty-informed threshold assessment for reducing misdiagnosis risks. The proposed framework can be extended to further developments on more MBFD methods in power electronic converters.

APPENDIX

The discrete voltage equations of upper and lower arms for the MMC can be expressed as

$$i_p^{k+1} = i_p^k + \frac{T_s}{L_0}\left(\frac{U_{dc}}{2} - u_p - u_{ac}\right) \tag{A1}$$

$$i_n^{k+1} = i_n^k + \frac{T_s}{L_0}\left(\frac{U_{dc}}{2} - u_n + u_{ac}\right) \tag{A2}$$

Introducing disturbance term d_1 and d_2 containing the actual inductance in the upper and lower arms, (A3) and (A4) are described by the following

$$i_p^{k+1} = i_p^k + \frac{T_s}{L_0}\left(\frac{U_{dc}}{2} - u_p - u_{ac}\right) + T_s d_1 \tag{A3}$$

$$i_n^{k+1} = i_n^k + \frac{T_s}{L_0}\left(\frac{U_{dc}}{2} - u_n + u_{ac}\right) + T_s d_2 \tag{A4}$$

where

$$d_1 = \left(\frac{1}{\tilde{L}_p} - \frac{1}{L_0}\right)\left(\frac{U_{dc}}{2} - u_p - u_{ac}\right),$$

$$d_2 = \left(\frac{1}{\tilde{L}_n} - \frac{1}{L_0}\right)\left(\frac{U_{dc}}{2} - u_n + u_{ac}\right).$$

Then, d_1 and d_2 can be estimated by the observer which is given by

$$\begin{cases} \hat{d}_1 = (1-\lambda) i_p^k - z_1^k \\ \hat{d}_2 = (1-\lambda) i_n^k - z_2^k \\ z_1^{k+1} = z_1^k + (1-\lambda)\left[\frac{1}{L_0}\left(\frac{U_{dc}}{2} - u_p - u_{ac}\right) + \hat{d}_1)\right] \\ z_2^{k+1} = z_2^k + (1-\lambda)\left[\frac{1}{L_0}\left(\frac{U_{dc}}{2} - u_n + u_{ac}\right) + \hat{d}_2\right)\right] \end{cases} \tag{A5}$$

where $\hat{d}$ is the estimated value of d, z is the state variable of the observer, and $|\lambda| < 1$ is the gain.

Therefore, the upper and lower arm inductance can be estimated by

$$\begin{cases} \hat{L}_p = \frac{L_0(U_{dc}/2 - u_p - u_{ac})}{\hat{d}_1 L_0 + U_{dc}/2 - u_p - u_{ac}} \\ \hat{L}_n = \frac{L_0(U_{dc}/2 - u_n + u_{ac})}{\hat{d}_1 L_0 + U_{dc}/2 - u_n + u_{ac}} \end{cases} \tag{A6}$$

REFERENCES

[1] C. Wang, A. Ali, and F. Blaabjerg, "Composition and control of a new type of hybrid voltage-source converter based on DRUs and FB-MMC for large-scale offshore wind power integration and transmission," *IEEE Trans. Power Electron.*, vol. 39, no. 5, pp. 5721–5732, May 2024.

[2] Q. Gui, H. Fehr, and A. Gensior, "Energy control of modular multilevel converters for drive applications at low frequency using general averaging," *IEEE Trans. Power Electron.*, vol. 39, no. 5, pp. 5239–5256, May 2024.

[3] Y. Jin et al., "A novel detection and localization approach of open-circuit switch fault for the grid-connected modular multilevel converter," *IEEE Trans. Ind. Electron.*, vol. 70, no. 1, pp. 112–124, Jan. 2023.

[4] H. Wang, Y. Li, A. Wijesekera, G. J. Kish, and Q. Zhao, "Switch open-circuit fault detection and localization for modular multilevel converters based on signal synthesis," *IEEE Trans. Emerg. Sel. Topics Power Electron.*, vol. 11, no. 5, pp. 5391–5404, Oct. 2023.

[5] S. Kiranyaz, A. Gastli, L. Ben-Brahim, N. Al-Emadi, and M. Gabbouj, "Real-time fault detection and identification for MMC using 1-D convolutional neural networks," *IEEE Trans. Ind. Electron.*, vol. 66, no. 11, pp. 8760–8771, Nov. 2019.

[6] F. Rojas, C. Jerez, C. M. Hack, O. Kalmbach, J. Pereda, and J. Lillo, "Faults in modular multilevel cascade converters-part II: Fault tolerance, fault detection & diagnosis and system reconfiguration," *IEEE Open J. Ind. Electron. Soc.*, vol. 3, pp. 594–614, 2022.

[7] D. Coronado and K. Fischer, "Condition monitoring of wind turbines: State of the art, user experience and recommendations," *Fraunhofer Inst. Wind Energy Energy Syst. Technol.*, Tech. Rep., Jan. 2015. [Online]. Available: https://www.vgb.org/vgbmultimedia/383_Finalreport-p-9786.pdf

[8] H. Badihi, Y. Zhang, B. Jiang, P. Pillay, and S. Rakheja, "A comprehensive review on signal-based and model-based condition monitoring of wind turbines: Fault diagnosis and lifetime prognosis," *Proc. IEEE*, vol. 110, no. 6, pp. 754–806, Jun. 2022.

[9] R. Venkataraman, P. Seiler, M. Lukátsi, and B. Vanek, "Reliability assessment of actuator architectures for unmanned aircraft," *J. Aircr.*, vol. 54, no. 3, pp. 955–966, May 2017.

[10] C. Wang, Z. Zheng, K. Wang, and Y. Li, "Fault detection and tolerant control of IGBT open-circuit failures in modular multilevel matrix converters," *IEEE J. Emerg. Sel. Topics Power Electron.*, vol. 10, no. 6, pp. 6714–6727, Dec. 2022.

[11] X. Chen, J. Liu, Z. Deng, S. Song, S. Du, and D. Wang, "A diagnosis strategy for multiple IGBT open-circuit faults of modular multilevel converters," *IEEE Trans. Power Electron.*, vol. 36, no. 1, pp. 191–203, Jan. 2021.

[12] W. Zhou, J. Sheng, H. Luo, W. Li, and X. He, "Detection and localization of submodule open-circuit failures for modular multilevel converters with single ring theorem," *IEEE Trans. Power Electron.*, vol. 34, no. 4, pp. 3729–3739, Apr. 2019.

[13] D. Zhou, S. Yang, and Y. Tang, "A voltage-based open-circuit fault detection and isolation approach for modular multilevel converters with model predictive control," *IEEE Trans. Power Electron.*, vol. 33, no. 11, pp. 9866–9874, Nov. 2018.

[14] C. Zhang, G. Song, T. Wang, and X. Dong, "An improved non-unit traveling wave protection method with adaptive threshold value and its application in HVDC grids," *IEEE Trans. Power Del.*, vol. 35, no. 4, pp. 1800–1811, Aug. 2020.

[15] S. He, W. Tian, R. Zhu, Y. Zhang, and S. Mao, "Electrical signature analysis for open-circuit faults detection of inverter with various disturbances in distribution grid," *IEEE Trans. Ind. Inf.*, vol. 19, no. 7, pp. 8351–8361, Jul. 2023.

[16] T. Xue, S. X. Ding, M. Zhong, and D. Zhou, "An integrated design scheme for SKR-based data-driven dynamic fault detection systems," *IEEE Trans. Ind. Inform.*, vol. 18, no. 10, pp. 6828–6839, Oct. 2022.

[17] Z. Geng and M. Han, "Fault localization strategy for modular multilevel converters in rectifier mode under submodule switch open-circuit failure," *IEEE Trans. Circuits Syst. II: Exp. Briefs*, vol. 67, no. 12, pp. 3222–3226, Dec. 2020.

[18] Y. Zhang, H. Wang, Z. Wang, F. Blaabjerg, and M. Saeedifard, "Mission profile-based system-level reliability prediction method for modular multilevel converters," *IEEE Trans Power Electron.*, vol. 35, no. 7, pp. 6916–6930, Jul. 2020.

[19] N. Rashidi, Q. Wang, R. Burgos, C. Roy, and D. Boroyevich, "Multi-objective design and optimization of power electronics converters with uncertainty quantification—Part I: Parametric uncertainty," *IEEE Trans. Power Electron.*, vol. 36, no. 2, pp. 1463–1474, Feb. 2021.

[20] Y. Zhang, H. D. Hwang, Y. M. Gu, J. Kim, F. Blaabjerg, and H. Wang, "Physical model based monte carlo early failure analysis of a switching mode power supply used in HVDC transmissions," in *Proc. CIGRE Session*, Paris, 2022, pp. 1–8.

[21] H. He and E. A. Garcia, "Learning from imbalanced data," *IEEE Trans. Knowl. Data Eng*, vol. 21, no. 9, pp. 1263–1284, Sep. 2009.

[22] N. Jardine and C. J. van Rijsbergen, "The use of hierarchic clustering in information retrieval," *Inf. Storage Retrieval*, vol. 7, no. 5, pp. 217–240, 1971.

[23] N. R. Mehrabadi, R. Burgos, C. Roy, and D. Boroyevich, "Power electronics modeling and design: Using parametric and model-form uncertainty quantification to assess predictive accuracy of power converter models," *IEEE Power Electron. Mag.*, vol. 4, no. 4, pp. 44–52, Dec. 2017.

[24] D. A. Douglass, "Potential transformer accuracy at 60 Hz voltages above and below rating and at frequencies above 60 Hz," *IEEE Trans. Power App. Syst.*, vol. PAS-100, no. 3, pp. 1370–1375, Mar. 1981.

[25] LEM, "DVC 1000," Jan. 2023. [Online]. Available: https://www.lem.com/sites/default/files/products_datasheets/dvc_1000_v3.pdf

[26] LEM, "HAH1DRW 100-S/SP5," Oct. 2020. [Online]. Available: https://www.lem.com/sites/default/files/products_datasheets/hah1drw_s_sp5_public_v0.pdf

[27] *IEEE Recommended Practice for the Design and Application of Power Electronics in Electrical Power Systems*, IEEE Std. 1662-2023 (Revision of IEEE Std 1662-2016), pp. 1–70, 2024.

[28] K.-S. Kim and K.-H. Rew, "Reduced order disturbance observer for discrete-time linear systems," *Automatica*, vol. 49, no. 4, pp. 968–975, 2013.

[29] A. P. Bradley, "The use of the area under the ROC curve in the evaluation of machine learning algorithms," *Pattern Recognit.*, vol. 30, no. 7, pp. 1145–1159, 1997.

[30] B. Li, S. Shi, B. Wang, G. Wang, W. Wang, and D. Xu, "Fault diagnosis and tolerant control of single IGBT open-circuit failure in modular multilevel converters," *IEEE Trans. Power Electron.*, vol. 31, no. 4, pp. 3165–3176, Apr. 2016.

[31] S. Shao, P. W. Wheeler, J. C. Clare, and A. J. Watson, "Fault detection for modular multilevel converters based on sliding mode observer," *IEEE Trans. Power Electron.*, vol. 28, no. 11, pp. 4867–4872, Nov. 2013.